Introduction

The accuracy and efficiency of full-waveform inversion (FWI) relies on the quality of wavefield modeling. In order to calculate both spatial and time derivatives needed for numerical solutions to a wave equation, one may use the finite-difference method (FDM), which replaces derivatives with numeric approximations of limited accuracy, due to its simple implementation and reduced computational cost.

The accuracy of FDM depends on spatial and temporal discretization. Fine spatial grids increase the precision of the numeric derivatives while proportionally increasing the computational cost. On the other hand, coarse grids reduce the modeling costs, but introduce numerical errors in the simulations causing phase distortions in the modeled wavefield. Additionally, large time steps may cause instabilities of the wavefield extrapolation, thus hampering FWI. Therefore, it is important to determine appropriate grid sizes in order to avoid numerical distortions and instabilities and increase the computational efficiency, while assuring modeling accuracy.

The CFL condition (Courant et al., 1967) defines an upper time step limit for stable finite-difference solutions of partial differential equations. If this condition is violated, large errors are produced during the simulation. The CFL condition is directly related to the spatial grid size and to the maximum velocity of the medium. Therefore, the space and time discretization should not be arbitrarily chosen as they depend on the medium properties. During FWI, the gradient of the objective function based on the misfit between observed and predicted data may lead to velocity updates that violate the CFL condition or cause undesirable dispersion, which results in inaccurate models.

We propose to avoid numerical instabilities during the inversion by explicitly incorporating a stability constraint into the FWI objective function, based on a probability density function (PDF), defining the range of parameters for which the wavefield simulations remain stable. We use the formulation proposed by Aragao and Sava (2020a,b) in order to recover models that do not violate the CFL condition or create numerical dispersion. The performance of the proposed methodology is illustrated with synthetic elastic examples.

Method

We consider the isotropic elastic wave equation

$$\ddot{\mathbf{u}} - V_P^2 \left[\nabla(\nabla \cdot \mathbf{u})\right] + V_S^2 \left[\nabla \times (\nabla \times \mathbf{u})\right] = \mathbf{f}, \tag{1}$$

where $\mathbf{u}(e,\mathbf{x},t)$ is the elastic wavefield, $\mathbf{f}(e,\mathbf{x},t)$ is the source function, and e, $\mathbf{x}$ and t are, respectively, the experiment index, space coordinates and time. The model parameters, V_P and V_S, are P- and S-waves velocities, respectively. We solve the full-waveform inversion problem by minimizing an objective function $\mathscr{J}(\mathbf{u},V_P,V_S)$ consisting of a term that estimates the misfit between the predicted and observed data $\mathscr{J}_D(\mathbf{u},V_P,V_S)$ using the L-2 norm, and a stability penalty $\mathscr{J}_S(V_P,V_S)$ that prevents numerical instabilities and grid dispersion during the FWI process.

During the numerical modeling, the phase velocity becomes a function of the spatial grid and it may be different than the true velocity when using an insufficient number of grid points per wavelength, thus affecting the high-frequency content of the data and creating numerical dispersion (Boore, 1972; Alford et al., 1974). For implementing fourth-order finite difference methods, if the grid size in any dimension is coarser than a quarter of the minimum wavelength, numerical grid dispersion may occur, leading to wavefield extrapolation instability. Additionally, numerical instabilities may also occur when one uses a propagation timestep inconsistent with the CFL condition (Courant et al., 1967):

$$\Delta t \leq \mathscr{C} \frac{\Delta x}{V_{max}}, \tag{2}$$

where Δt represents the time step, Δx represents the spatial grid in any direction, $\mathscr{C}$ is the Courant number and V_{max} corresponds to the maximum velocity. The CFL condition is a necessary condition for avoiding dispersion when numerically solving partial differential equations.

Furthermore, for multiparameter inversion that uses only the data misfit, model parameter updates may produce unphysical models (e.g., negative velocities), which also lead to instabilities in wavefield extrapolation. In order to purposefully prevent numerical instabilities and numerical dispersion, we design a stability penalty $\mathscr{J}_S$ in the elastic FWI (EFWI) objective function. We adapt the formulation of the probabilistic petrophysical constraint proposed by Aragao and Sava (2020a,b), which is not calculated in the physical space domain, but in the space formed by the model parameters. We define a probability density function (PDF) that represents the range of model parameters for which wavefield simulations remain stable. The PDF is represented by coordinates $\mathbf{p} = [V_{Pp}, V_{Sp}]$ and probability density $b(\mathbf{p})$, such that $b = 0$ for combinations of parameters that cause wavefield simulation instability. Representing the elastic model components by the vector $\mathbf{m} = [V_P, V_S]$, we define the stability penalty as

$$\mathscr{J}_S = a \sum_{\mathbf{m}} D(\mathbf{m}), \tag{3}$$

such that the scalar parameter a determines the relative strength of the stability term in the objective function and $D(\mathbf{m})$ represents the distance from a particular combination of model parameters $\mathbf{m}$ to the entire distribution given by

$$\frac{1}{D(\mathbf{m})} = \sum_{\mathbf{p}} \frac{b(\mathbf{p})}{\|\mathbf{m}-\mathbf{p}\|_2}. \tag{4}$$

The value of $\mathscr{J}_S$ is determined by the distance to high probabilities in the model parameter space, i.e., by the distance to the combinations of V_P and V_S that make wavefield extrapolation stable. Therefore, outside the stability region defined by the PDF, the gradient of $\mathscr{J}_S$ explicitly forces the models towards the stable region. For points $\mathbf{m}(\mathbf{x}) = \{V_P(\mathbf{x}), V_S(\mathbf{x})\}$ inside the stability region, the data misfit $\mathscr{J}_D$ fully controls the total gradient (Aragao and Sava, 2020a).

Examples

Gaussian Anomalies

The synthetic models depicted in Figure 1 contain two positive Gaussian anomalies centered at $(1.2, 0.75)$ and $(1.2, 1.75)$ km. There are 40 vertical displacement sources in a well at $x = 0.05$ km and a line of geophones at $x = 2.35$ km. For this experiment, we use the following parameters: $f_{max} = 15$ Hz; $\lambda_{min} \approx 33.3$ m; and the minimum velocity for the S-wave and maximum velocity for the P-wave are, respectively, $V_{Smin} = 500$ m/s and $V_{Pmax} = 2000$ m/s. Therefore, the maximum spatial grid is 8 m and, for $\mathscr{C} = 0.5$, the time step needs to be smaller than 0.0023 s.

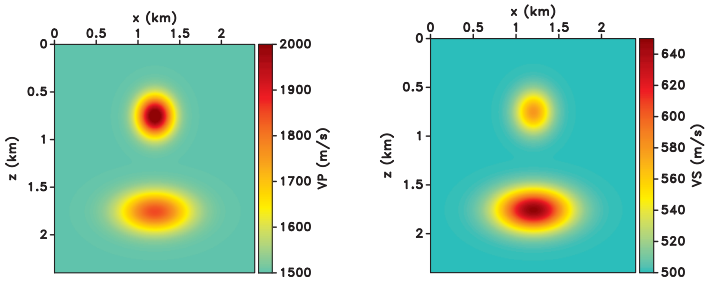

Figure 1 *Synthetic models with two positive Gaussian anomalies for the V_P and V_S models.*

For $\Delta x = 8$ m and $\Delta t = 0.002$ s, the inversion is stable when velocities are in the range $[480, 2000]$ m/s, which conforms to the true models (Figure 1). Inverted velocities outside this range produce wrong models and also cause wavefield simulation instabilities. Therefore, this example illustrates how we can avoid numerical dispersion and also prevent the inversion from generating incorrect models by using the stability penalty, which constrains the range of updated velocities. We start the inversion with a model with constant $V_P = 1500$ m/s and $V_S = 500\,m/s$.

Considering the range of velocities for which the wavefield simulations are stable, the inversion becomes unstable when we have V_S updates below -20 m/s or when V_P updates above 500 m/s. Therefore, we

define a PDF for calculating the stability penalty consisting of the distribution shown in Figure 2a. Note that the probability density is zero for velocities that produce wave propagation instability. Figure 2b displays the distance $D(\mathbf{m})$ and the gradient of $D(\mathbf{m})$, which are both zero in the region of stability. If the inverted velocities are inside the range defined by the PDF (Figure 2a), the data misfit $\mathscr{J}_D$ fully controls the inversion gradient as the gradients of $\mathscr{J}_S$ are zero. Otherwise, the stability constraint produces a gradient that drives the updated models to the region of stability defined by the PDF.

Without the stability constraint, we observe numerical dispersion in the inversion after few iterations. The inversion updates in Figure 3 show that, without imposing stability constraints, the V_S model has updates smaller than -20 m/s, producing velocities that are smaller than 480 m/s, thus causing wavefield extrapolation instability. Additionally, the inversion that uses just the data misfit produces negative anomalies (Figure 3) at the locations of the positive anomalies of the true models (Figure 1). Therefore, inversion based only in $\mathscr{J}_D$ produces wrong velocity models in addition to numerical dispersion. When we include the stability constraints into the inversion objective function, inversion proceeds without any instability. The inversion updates (Figure 4) demonstrate that the stability constraint secures the FWI stability and efficiency.

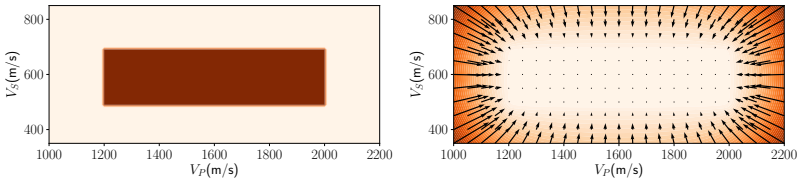

(a) (b)

Figure 2 *(a) Example of a PDF consisting of boxcar function representing the range of velocities in which the forward simulations remain stable. (b) The distance $D(\mathbf{m})$ and its gradient.*

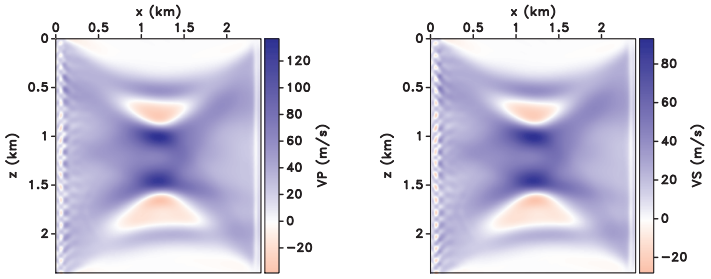

Figure 3 *Inversion updates for the V_P and V_S models using the objective function $\mathscr{J}_D$ after few iterations, right before numerical instability occurs.*

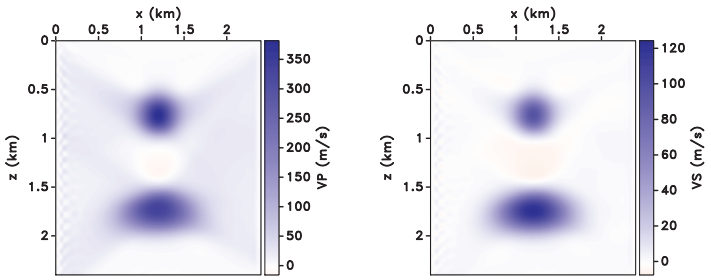

Figure 4 *Inversion updates for the V_P and V_S models using the objective function $\mathscr{J}_D + \mathscr{J}_S$ after 50 iterations.*

Marmousi model

The second synthetic example uses a portion of the Marmousi 2 model (Martin et al., 2002). Figure 5a shows the correct V_P and V_S models. We simulate a multicomponent ocean bottom seismic survey (OBS) with a line of receiver at the water bottom ($z = 0.2$ km) and 100 evenly spaced pressure sources located at $z = 0.05$ km. Figure 5b shows the initial V_P and V_S models.

Without the stability penalty, the inversion becomes unstable after 3 iterations. The updated models are in Figure 5c, showing that V_S has negative values, which prevent further updates. Then, conventional inversion is not able to produce long-wavelength updates which deteriorates the quality of the recovered models.

The stability penalty eliminates this problem. The recovered models after 50 iterations are shown in Figure 5d. Even though the recovered V_P and V_S models are contaminated with high-wavenumber artifacts in addition to the artifacts due to the inherent interparameter cross-talk of EFWI, the inversion delivers long-wavelength updates and produces high resolution models. In order to further enhance the quality of the inverted models, one can also include petrophysical constraints or a regularization term in the objective function.

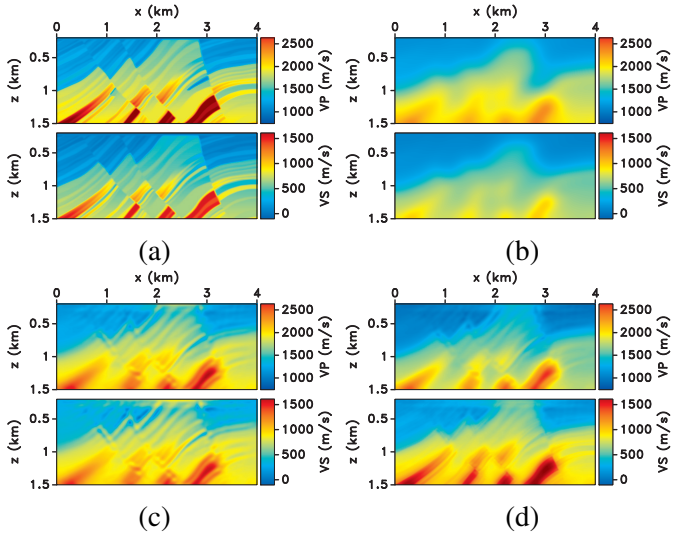

Figure 5 *Marmousi 2 V_P and V_S models: (a) true, (b) initial, (c) recovered using objective function $\mathscr{J}_D$, (d) recovered using the objective function $\mathscr{J}_D + \mathscr{J}_S$.*

Conclusions

We develop a strategy for incorporating a stability constraint into elastic full-waveform inversion through a penalty term that defines the range of velocities for which wave propagation is stable when using the finite-difference method. When the updated models are inside the stability region, which is defined by a probability density function, the inversion is fully controlled by the misfit between the observed and predicted data. We demonstrate that imposing this penalty avoids numerical dispersion and instabilities during wavefield simulation. Through synthetic examples, we verify the effectiveness of the proposed methodology in leading inversion towards an accurate solution, while preventing updates that hamper the accuracy and stability of the finite difference method.

References

Alford, R.M., Kelly, K.R. and Boore, D.M. [1974] Accuracy of finite-difference modeling of the acoustic wave equation. *Geophysics*, **39**, 834–842.

Aragao, O. and Sava, P. [2020a] Elastic full-waveform inversion probabilistic petrophysical model constraints. *Geophysics*, **85**, R101–R111.

Aragao, O. and Sava, P. [2020b] Elastic full waveform inversion with probabilistic petrophysical clustering. *Geophysical Prospecting*, Advance online publication. doi:10.1111/1365–2478.12910.

Boore, D.M. [1972] Finite Difference Methods for Seismic Wave Propagation in Heterogeneous Materials. *Methods in Computational Physics: Advances in Research and Applications*, **11**, 1–37.

Courant, R., Friedrichs, K. and Lewis, H. [1967] On the partial difference equations of mathematical physics. *IBM Journal of Research and Development*, **11**, 215–234.

Martin, G., Marfut, K. and Larsen, S. [2002] Marmousi-2, an updated model for the investigation of avo in structurally complex areas. In: *SEG Technical Program Expanded Abstracts*. 2478–2482.